PCCP

PAPER

View Article Online
View Journal | View Issue

Cite this: *Phys. Chem. Chem. Phys.*, 2015, **17**, 414

Interaction of magnetic nanoparticles with phospholipid films adsorbed at a liquid/liquid interface

C. I. Cámara,[a] L. M. A. Monzón,*[b] J. M. D. Coey[b] and L. M. Yudi*[a]

Received 2nd October 2014,
Accepted 28th October 2014

DOI: 10.1039/c4cp04464a

www.rsc.org/pccp

The interaction of Co hexagonal magnetic nanoparticles (MNPs) with distearoyl phosphatidyl glycerol (DSPG) and distearoyl phosphatidic acid (DSPA) films adsorbed at a water/1,2-dichloroethane interface is studied employing cyclic voltammetry (CV), electrochemical impedance spectroscopy (EIS), capacity curves and interfacial pressure–area isotherms. DSPA and DSPG adsorb at the interface forming homogenous films and producing a blocking effect on the transfer process of tetraethyl ammonium (TEA^+), used as a probe cation. In the presence of Co NPs this effect is reversed and the reversible transfer process for TEA^+ is reestablished, to a greater or lesser extent depending on the structuration of the film. Co–DSPA hybrid films have a homogeneous structure while Co-DSPG films present different domains. Moreover, the presence of Co on DSPA film modifies the partition coefficient of the organic electrolyte into the hydrocarbon layer.

1. Introduction

Magnetic nanoparticles (MNPs) are widely used in biomedicine due to their versatility. The most common applications are in biosensor platforms,[1] in drug or radioisotope delivery, as magnetic spacers of labeled cells, in tissue engineering,[2] as a contrast agent in magnetic resonance studies and in hyperthermia based-therapies[3–5] among others. Many applications are related to the interactions between MNPs and bio-membranes, and for this reason, the investigation of these interactions using different methodologies and bio-membrane models has gained great importance in the last few years.

Recently, it has been demonstrated that citric acid – adsorbed $CoFe_2O_4$ nanoparticles modify the biological membranes as well as their artificial models, more than bare $CoFe_2O_4$, due to the formation of nanoparticle aggregates in lipidic structures.[6] On the other hand, it has also been shown that silica coated iron oxide nanoparticles produce a decrease of 25% in the elasticity modulus of membranes.[7] Besides, studies of the interaction of hydrophobic magnetic nanoparticles with saturated and unsaturated phospholipids have been reported, showing that the nanoparticles modify the compression isotherms and the topography of the films, producing an expansion of the monolayer for unsaturated phospholipids and a compression effect for saturated ones.[8] The behavior of phospholipids at liquid/liquid interfaces and their interactions with metallic nanoparticles and polyelectrolytes have been extensively described,[9–12] but only scarce information can be found related to the electrochemical behavior of MNPs in phospholipid films adsorbed at liquid/liquid interfaces.

In the present work we evaluate the effect of Co MNPs on the interfacial structure and permeability of DSPA and DPSG films. These studies were accomplished using cyclic voltammetry (CV), electrochemical impedance spectroscopy (EIS) and capacity curves at liquid/liquid interfaces as well as interfacial pressure–area isotherms.

2. Materials and methods

CV and EIS were used to characterize the film of MNPs and MNPs/phospholipids at the interface, using a conventional glass cell (0.94 cm^2 interfacial area) with a four-electrode configuration.[11]

The base electrolyte solutions were 10.0 mM $CaCl_2$ (p.a. grade) in ultra-pure water and 10.0 mM tetraphenylarsoniumtetrakis (4-chloro phenyl) borate (TPhAsClTPhB) in 1,2-dichloroethane (Dorwill p.a.). The pH of the aqueous solution was 5.00.

[a] *INFIQC (CONICET-Universidad Nacional de Córdoba), Departamento de Fisicoquímica, Facultad de Ciencias Químicas, Ala 1, Pabellón Argentina, Ciudad Universitaria, 5000 Córdoba, Argentina. E-mail: mjudi@fcq.unc.edu.ar; Fax: +54-0351-4334188; Tel: +54-0351-5353866*

[b] *School of Physics, Trinity College Dublin, Dublin 2, Ireland. E-mail: aranzazl@tcd.ie*

The electrochemical cell used was

		TPAsCl	TPhAsClTPhB	$CaCl_2$		
Ag	AgCl	10.00 mM	10.00 mM	10.00 mM	AgCl	Ag
		(w′)	(o)	(w)		

Working interface

Co MNPs were synthesized as described in,[13] employing 9.00 mL of dioctylether (Sigma-Aldrich), 0.50 mL of oleic acid (Sigma-Aldrich) and 0.20 mL of oley amine (Sigma-Aldrich). The mixture was agitated at 80 °C for 1 h, under Ar. Then 0.0470 g of $CoCl_2$ was added under constant agitation at T = 150 °C. After dissolution of the salt, 2.00 mL of lithium triethylborohydride ($LiEt_3BH$, Sigma-Aldrich) was injected and the temperature was increased to 200 °C for 30 min. Later, the mixture was allowed to stand for 2 h at room temperature and then ethanol was added to precipitate Co NPs, which were separated and washed with acetone. After the synthesis, Co MNPs were characterized by magnetization experiments, performed on a Quantum Design SQUID 5T magnetometer at room temperature; Fourier transform infrared spectroscopy (FT-IR spectra), performed on a Bruker IFS28 spectrophotometer; scanning electron microscopy images (SEM), taken on a Zeiss Auriga microscopy; energy dispersive X-ray spectroscopy (EDS), performed on a Carl Zeiss microscope FE-SEM Sigma; and X-ray diffraction (XRD), employing a PANalytical X'pert Pro X system with Cu Kα (λ = 1514.1 pm) radiation, X-ray source and an X'celerator IP detector. The magnetization loops for Co MNPs showed a saturation magnetization (M_s) equal to 45 A m^2 Kg^{-1} and a coercivity, $\mu_0 H_c$ = 25 mT, indicating that Co MNPs are still magnetized when the external magnetic field is switched off (the remanence, M_r, is 28% of M_s). XRD patterns presented several reflections arising from the 100, 002, 101, 102, 110 and 112 planes of the hexagonal structure. For randomly oriented hcp Co powders, the intensity of the 101 reflection is much stronger than the intensity of the 002 or 100, whereas here the XRD pattern of Co nanopowder showed that the peak corresponding to the 002 reflection has a much stronger intensity than the rest. This indicates that the Co nanoparticles have a preferential orientation along the *c*-axis driven by the magnetocrystalline anisotropy of hcp Co. The observed room temperature coercivity of these samples suggests the existence of hcp cobalt. SEM images showed an elongated structure with an average crystal size of 25 nm. Given the non-zero magnetization of Co NPs, during the synthesis, they tend to align their magnetic dipoles along a longitudinal direction, giving rise to needle or rod-like shapes. EDS and FT-IR experiments were performed to characterize the surfactants adsorbed on the MNP surface. EDS spectra demonstrated the presence of cobalt (Co), carbon (C) and oxygen (O), indicating the presence of hydrocarbon chains with functional groups containing O at MNP surfaces. Taking into account that oleic acid was added, as a stabilizing agent, during the synthesis of Co MNPs, it can be concluded that these MNPs are derivatized with this acid at their surfaces. This was corroborated by FT-IR spectra obtained from solid samples incorporated in KBr pellets. Sharp peaks between 1300 and 1500 cm^{-1} were observed, which can be attributed to carboxylic groups attached to Co, or to the signal of carbonyl groups in the acid, shifted toward lower wave numbers with respect to the signal of the carboxylic acid in solution. Other important peaks were found in the region between 3000–2700 cm^{-1}, which correspond to the stretching of the C–H bond on methyl groups in the hydrocarbon tails. Based on these results, the presence of carboxylic groups on Co MNPs was confirmed.

The MNP dispersion was prepared in ethylic alcohol, at a concentration of 0.730 g mL^{-1} and sonicated for 10 min before use.

Distearoyl phosphatidic acid (DSPA) and distearoyl phosphatidyl glycerol (DSPG) were of analytical grade (Sigma-Aldrich). A solution 1.00 mM of DSPA or DSPG in 1 : 2 methanol : chloroform was prepared. In order to form the phospholipid film, 100 μL of DSPA or DSPG solutions were injected, at the liquid/liquid working interface, formed between TPhAsClTPhB and $CaCl_2$ solutions, after both phases were brought into contact in the electrochemical cell. 60 min was required, since the injection of the phospholipid solution, to obtain an invariant and reproducible voltammetric response, indicating that a stable film has been formed. The mixtures DSPA:Co or DSPG:Co were performed mixing 100 μL of DSPA or DSPG solutions with different volumes (0–150 μL) of MNP dispersion.

Voltammograms were obtained using an aqueous solution of 0.50 mM tetraethylammonium chloride (TEACl, Sigma). TEA^+ was employed as a probe ion, since its transfer, from the aqueous to the organic phase, is reversible and diffusion controlled.

CV was performed using a potentiostat with periodic current interruption for automatic elimination of solution resistance and a potential sweep generator (LyP Electrónica Argentina). EIS was carried out employing an electrochemical analyzer CHI C700. The data acquisition and processing were performed with ZPlot/Zview (Scribner Associates Inc.) program. The frequency range was 0.05–4000 Hz, the amplitude of the ac perturbation was 10 mV and the constant dc potential, E, was 0.450 V. Capacity (C) *vs.* E curves were recorded at the frequency value corresponding to the maximum of Bode plots (phase angle *vs.* frequency).

Surface pressure–molecular area isotherms were recorded with a mini-trough II from KSV Instruments Ltd (Helsinki, Finland). The surface tension was measured using the Wilhelmy plate method with a platinum plate. The aqueous subphase, contained in a Teflon trough (364 mm × 75 mm effective film area), was 10.00 mM $CaCl_2$, pH = 5.00.

To prepare DSPG and DSPA monolayers at the air/water interface, 50 μL of 0.550 mM DSPG or DSPA solution, in 1 : 2 methanol : chloroform, was carefully spread on the surface using a Hamilton micro-syringe. Before spreading DSPG or DSPA solutions, the subphase surface was cleaned by sweeping it with the Teflon barriers and then, any surface contaminant

was removed by suction from the interface. The cleaning of the surface was checked by recording an isotherm in the absence of phospholipids and verifying a surface pressure value lower than 0.20 mN m^{-1}. After spreading, the solvent was allowed to evaporate for 10 min, and then the film was compressed with two barriers, one on each side of the trough at a compression speed of 5 mm min^{-1} while the automatic measurement of the lateral surface pressure (π) was carried out. In the case of mixed DSPA:Co or DSPG:Co monolayers, solutions containing 50 μL of 0.550 M DSPG or DSPA and different volumes (4, 11 or 20 μL) of 0.73 g mL^{-1} Co MNP dispersion were spread on the surface.

All experiments were performed at 25 ± 1 °C using a HAAKE G. thermostat. At least two compression isotherms were registered under each condition and results with a typical area and collapse pressure errors of ±2 $Å^2$ and ±1 mN m^{-1} respectively were obtained.

The surface compression modulus κ (mN m^{-1}) was calculated from the compression isotherm as:

$$\kappa = -A \times \left(\frac{\partial \pi}{\partial A}\right)_T \quad (1)$$

where A is the area per molecule and π is the surface pressure in mN m^{-1}. The uncertainty of compression modulus was ±10 mN m^{-1}.

3. Results and discussion

Fig. 1a shows the voltammetric response corresponding to TEA^+ transfer across the bare interface (solid black line) and in the presence of the DSPG monolayer formed after 60 min of injecting 100 μL of 1.00 mM DSPG solution at the interface. The solid black line corresponds to the very well-known reversible diffusion controlled behavior of the TEA^+ transfer process across the bare liquid/liquid interface. A forward current peak at E_p = 0.400 V and the corresponding backward process with a peak to peak separation ΔE_p = 0.060 V can be observed. The peak current, I_p, is linear with $v^{1/2}$ over the whole range of sweep rates analyzed (not shown). If this response is compared with that obtained when the DSPG molecules are present at the interface, an important decrease in current and a shift of the positive peak potential towards more positive values can be noticed. These changes evidence a blocking effect of the layer on TEA^+ transfer, since it can be assumed that the transfer potential shift is due to the increase in Gibbs energy on transfer caused by the work of permeation of species across the film. However this effect decreases when Co MNPs are incorporated into the film, almost disappearing for the highest Co:DSPG relationship, recovering, under this condition, a voltammetric response close to the original one. This is a demonstration that Co MNPs produce disorder on the film or formation of bare

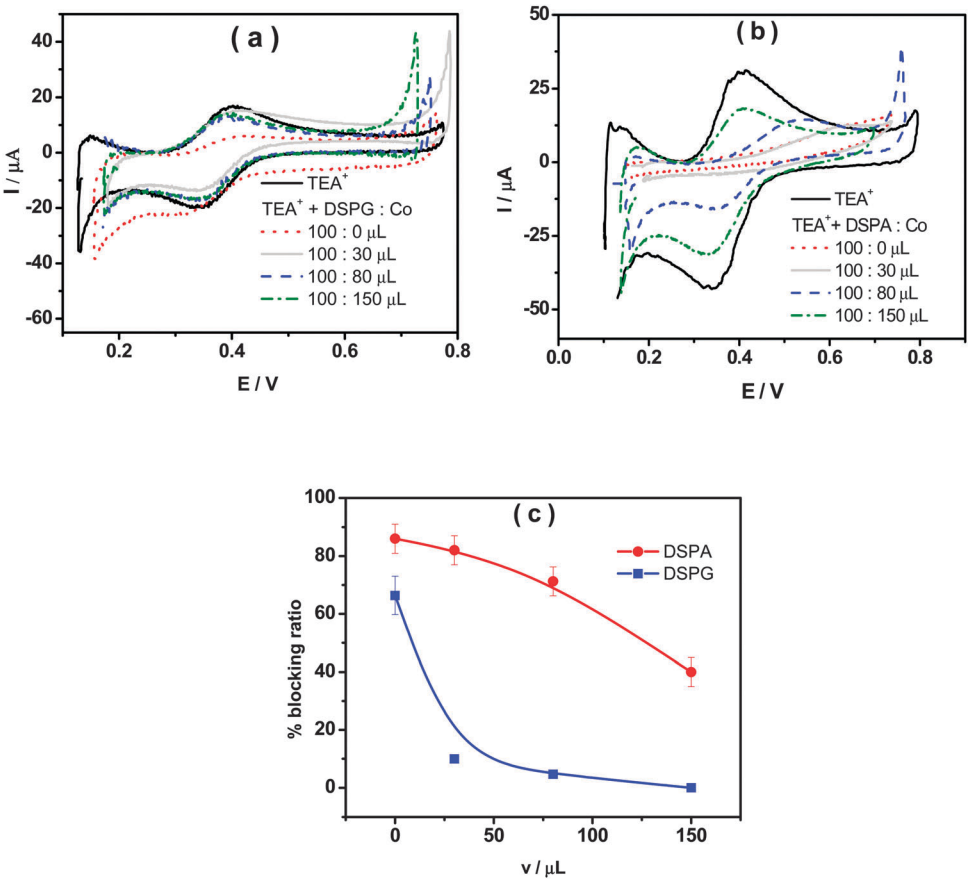

Fig. 1 Cyclic voltammograms for the TEA^+ transfer process across the liquid/liquid interface in the absence (—) or in the presence of phospholipid : Co mixtures (100 : x μL) for (a) DSPG and (b) DSPA. (c) The blocking ratio *vs.* volume of MNP solution in the mixtures DSPG : Co (■) or DSPA : Co (●).

zones (pores), minimizing its blocking effect on TEA^+ transfer. Quite similar results were obtained for DSPA films (Fig. 1b). In this case the presence of the film produces an almost complete blocking effect on the TEA^+ transfer process, showing its strong compactness. In this case, the TEA^+ reversible transfer process observed at $E = 0.400$ V completely disappears and a new process is evident at higher potential values ($E_p \cong 0.630$ V) without the corresponding negative peak. It has been demonstrated in a previous paper[14] that the positive peak at $E_p \cong 0.630$ V corresponds to the TEA^+ adsorption at the negative polar head groups of DSPA. This blocking effect also decreases in the presence of Co MNPs in the film, nevertheless, it is not reversed even for the highest Co:DSPA relationship. In this case, Ca^{2+} cations produce an important structuring effect on DSPA monolayers due to their strong interaction with the partially ionized anionic polar head groups of phospholipids which diminishes the lateral electrostatic repulsions as it has already been reported.[14] Under these conditions, Co MNPs are not able to totally disorganize the film, probably due to the partial impediment to penetrate into these very tightly compacted monolayers. Fig. 1c summarizes the results obtained for the effect of increasing Co:DSPX (X = G or A) relationship on the permeability of DSPA or DSPG films. For this purpose a blocking ratio percentage for each Co : DSPX relationship was calculated as:

$$\text{Blocking ratio} = \frac{\left(I^{TEA^+} - I^{TEA^+,FILM}\right)}{I^{TEA^+}} 100 \qquad (2)$$

where I^{TEA^+} and $I^{TEA^+,\,FILM}$ are the peak current values for the TEA^+ transfer process in the absence and in the presence of the film for each Co : DSPX ratio, respectively. As it can be noted, the Blocking ratio shows a sharp decrease to values close to 0% for DSPG films in the presence of the highest Co MNP concentration. Instead, a slight decrease of only 40% was obtained for DSPA for the highest Co : DSPA ratio.

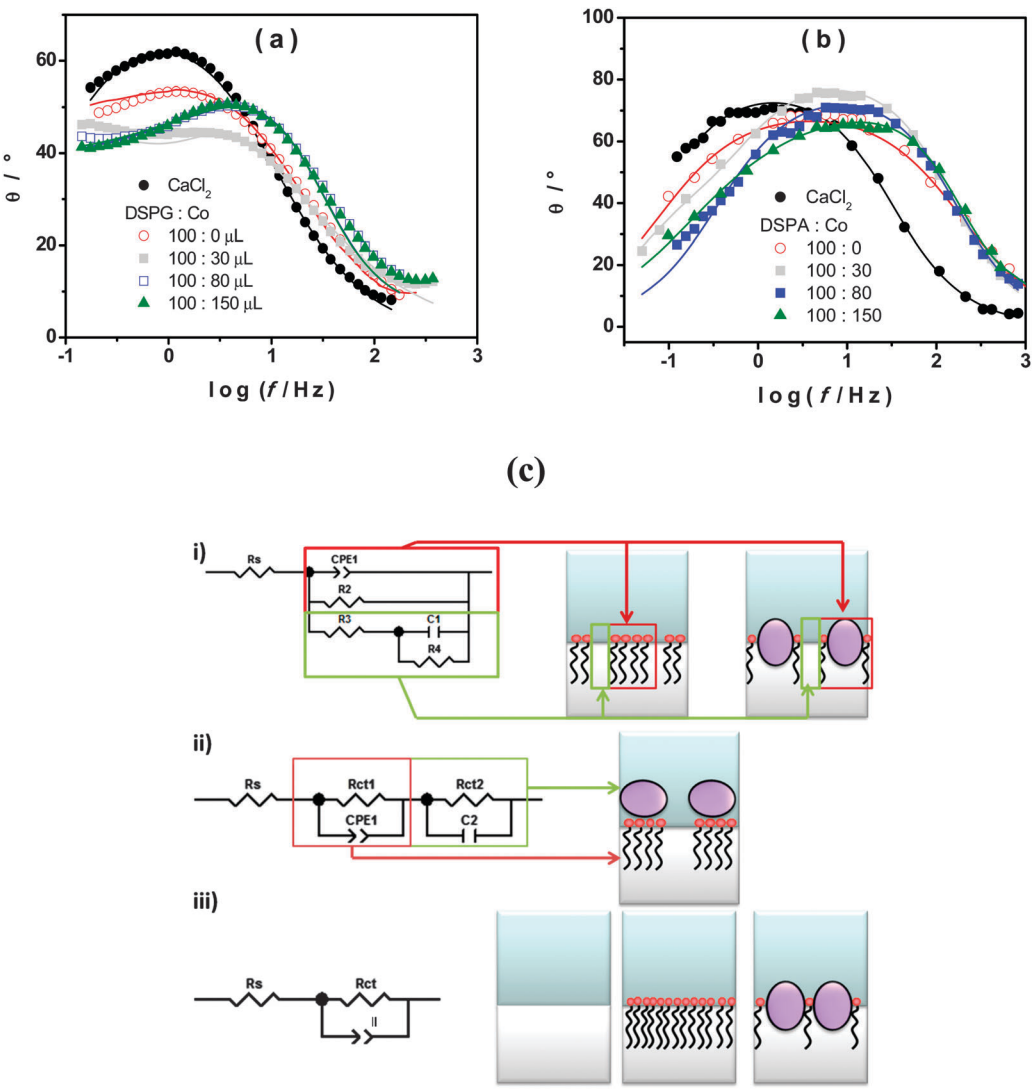

Fig. 2 Phase angle (θ) *vs.* log f in the absence (●) or in the presence of phospholipids : Co mixtures (100 : x μL) for (a) DSPG and (b) DSPA. (c) Equivalent circuits employed to fit EIS results and the corresponding interfacial models.

Summing up, the results shown above indicate that DSPG and DSPA monolayers have a blocking effect on TEA^+ transfer, but its structure and permeability can be altered by the presence of Co MNPs, which can expand the monolayer in greater or lesser extent depending on the polar head group of the phospholipid.

With the aim of evaluating the properties of DSPG and DSPA films in the presence of Co MNPs, EIS experiments were carried out. In these experiments no probe ion (TEA^+) was used. An ac perturbation of amplitude 10 mV and frequency scanned between 0.05 Hz to 3 kHz was applied to the interface at a dc potential E = 0.450 V. The EIS data were fitted with several equivalent circuits using the software ZPLOT/ZVIEW (Scribner Associates, Inc.). The schemes of equivalent circuits used in this analysis are shown in Fig. 2c. The circuit which best fits the experimental data depends on the composition of the film. Scheme (iii) is the Randles circuit where R_s is the solution resistance, CPE_{dl} is a constant phase element representing the double layer capacitance and R_{ct} is the charge transfer resistance. This model describes properly the behavior of the interface in the absence of any monolayer or in the presence of a homogeneous film coating completely the interface (as shown schematically in the drawing next to the circuit). In the last case, $CPE_{monolayer}$ is used instead of CPE_{dl} and R_{ct} is the charge transfer resistance across the monolayer. Scheme (i) represents the interface structure when the monolayer contains different domains with pore formation (see the drawing next to the circuit). CPE_1 and R_2 in the equivalent circuit correspond to the capacitance of the coated zones of the interface and the charge transfer resistance across the film respectively, while R_3, C_1 and R_4 are the solution resistance, the capacitance and charge transfer resistance at the pores, *i.e.* the uncoated zones. The circuit shown in scheme (ii) corresponds to films with layer differentiation, *i.e.* a layer of phospholipids underneath a layer of nanoparticles. In this case, CPE_1 and R_{ct1} represent the double layer capacity and the transfer resistance of the first layer, in the same way C_2 and R_{ct2} correspond to the second layer.

Fig. 2a and b show the Bode (θ, phase angle, *vs.* log$f$) plots obtained for the interface between $CaCl_2$ aqueous solution and TPhAsClTPhB organic solution with and without DSPG or DSPA, respectively in the absence and in the presence of different amounts of Co MNPs. Symbols represent the experimental data, while solid lines are the result of the best fitting. In the absence of the monolayer (•) the typical response corresponding to the Randles circuit is obtained. When DSPG or DSPA solutions are injected at the interface, in the absence of Co MNPs, the same Randles circuit fits the experimental data in both cases, but with lower CPE_{dl} ($CPE_{monolayer}$) values due to the presence of hydrocarbon chains at the interface (C values decrease from 2.9×10^{-5} F for the bare interface to 6.0×10^{-6} F when DSPA film is present at the interface). The same Randles circuit was used to fit the experimental data when Co MNPs were incorporated into the film of DSPA at any concentration, indicating that the monolayer structure is largely preserved. Nevertheless, subsequently lower R_{ct} values were obtained as the Co MNP amount in the film was increased, indicating that Co MNPs intercalate into the hydrocarbon chains generating a slight expansion of the monolayer, which also would explain the partial decrease in the blocking ratio of TEA^+ transfer observed in Fig. 1. In contrast, in the case of DSPG, two time constants are observed in Bode plots for DSPG : Co at the ratio 100 : 30. Under this condition, the circuit of scheme (ii) is the one which best fits the results, demonstrating the presence of adjacent layers of phospholipids and Co MNPs. On the other hand, the circuit in scheme (i) fits the results when the amount of Co MNPs in the film increases (ratios 100 : 50 and 100 : 80), indicating the presence of different domains: bare and covered zones. A possible explanation for this change in the film structuration could be the fact that, once the bilayer is formed and as the Co amount increases, DSPG molecules present at the interface reorganize themselves to form films containing Co MNPs mixed with DSPG molecules. In these films, the covered zones could be less than bare ones as Co MNP concentration increases and so, very few DSPG molecules would be present at the interface and no blocking effect is produced as observed in voltammetric experiments.

Fig. 3 shows the variation of interfacial capacity, C, at E = 0.450 V with the volume of Co MNP solution present in the DSPG:Co or DSPA:Co mixtures injected at the interface. C values were evaluated from EIS fitting. When MNPs are part of DSPG films, the bare domain capacity decreases with the MNP concentration at the interface, since the area of these domains decreases, indicating the incorporation of MNPs into these domains of the film, while the capacity of covered areas remains almost independent of MNP concentration. Decreasing capacity values with MNP volume were also obtained for DSPA films, although to a lesser extent than the effect observed for DSPG films, indicating lesser penetration of MNPs into these highly structured films.

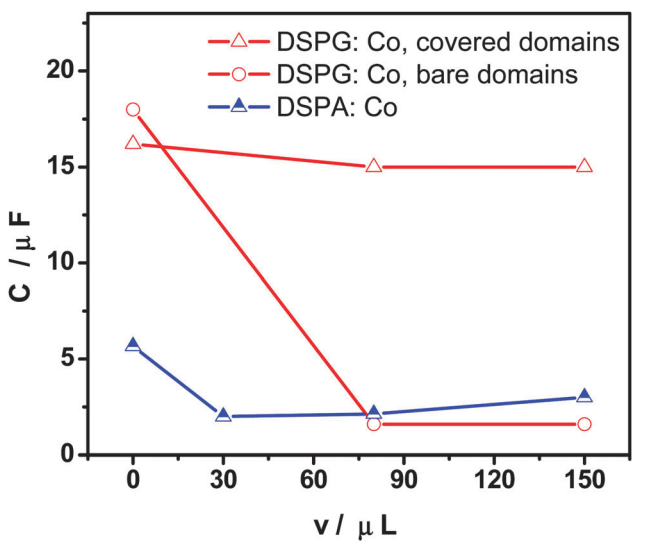

Fig. 3 Capacity (C) as a function of the injected volume of Co MNPs in the mixture phospholipids : Co (100 : x μL) for DSPG (empty symbols) and DSPA (half full symbols).

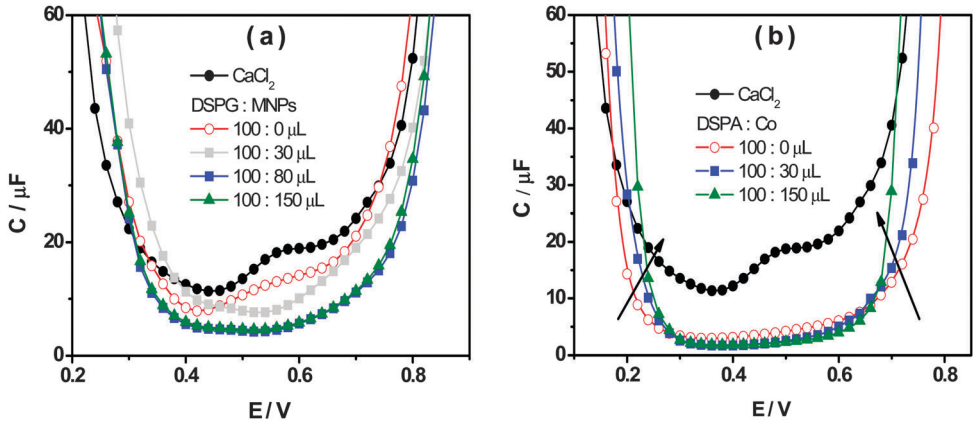

Fig. 4 Capacity as a function of the applied potential in the absence (●) and the presence of phospholipids : Co (100 : *x* μL) mixtures for (a) DSPG and (b) DSPA.

Fig. 4a and b show the interfacial capacity, *C*, *vs.* *E* plots for DSPG and DSPA films respectively, containing increasing amounts of Co MNPs. The curves corresponding to the bare interface, in the absence of any film, are also shown for comparison. These curves were measured at three frequency values, at the maximum in the plot of θ *vs.* log*f*. A general decrease of *C* values is evident when both, DSPG and DSPA, monolayers are formed, with respect to those corresponding to the bare interface, suggesting a decrease in the interfacial dielectric constant due to the presence of hydrocarbon chains. The capacity decreases further when the amount of MNPs in the film increases, which can be explained taking into account the decrease of bare areas. Moreover, the curves obtained for DSPA + MNP film, become narrower as the amount of MNPs in the film increases. Martins *et al.*[9] have attributed this effect to a change in the partition coefficient of ions from base electrolytes into the hydrocarbon region. The organic electrolyte partitions into the interfacial region occupied by the hydrocarbon chains (hc), the concentration of this electrolyte in hc, c_{hc}, depends on the partition coefficient, K_{hc}, and its concentration in the organic phase, $c_{hc} = K_{hc}c^{o}$. K_{hc}, in turn, depends on the degree of compaction of the film. The increase in Co MNP concentration produces a slight expansion of the DSPA monolayer, and consequently an increase in the K_{hc} value, which leads to more narrow capacity curves with respect to that obtained for pure DSPA monolayers. This expansion effect is consistent with the decrease in the blocking effect on TEA^{+} transfer observed in VC experiments with increasing concentrations of MNPs.

The surface pressure–area compression isotherms are shown in Fig. 5a and b for DSPG and DSPA monolayers, respectively, formed at the air/water interface in the absence and in the presence of different amounts of Co MNPs, using 10 mM $CaCl_2$ in the subphase.

In the absence of Co MNPs, both phospholipids show a change in the slope of the isotherm corresponding to the lift-off due to the gaseous-liquid condensed phase transition as described in ref. 11, 12, 15 and 16. The collapse pressures of monolayers are 54.6 mN m^{-1} and 55.7 mN m^{-1} for DSPG and DSPA respectively, with corresponding mean molecular areas of 0.370 nm^2 and 0.390 nm^2. No significant changes in the surface pressure–area isotherms are visible when phospholipids:Co mixtures are spread on the subphase, except for a slight shift of the curves towards smaller areas, probably due to the removal of some phospholipid molecules, together with Co MNPs, out of the monolayer, since in this figure the area is given in terms of area per phospholipid molecule. It is important to remark that Co MNPs, due to their high hydrophilicity, do not show surface

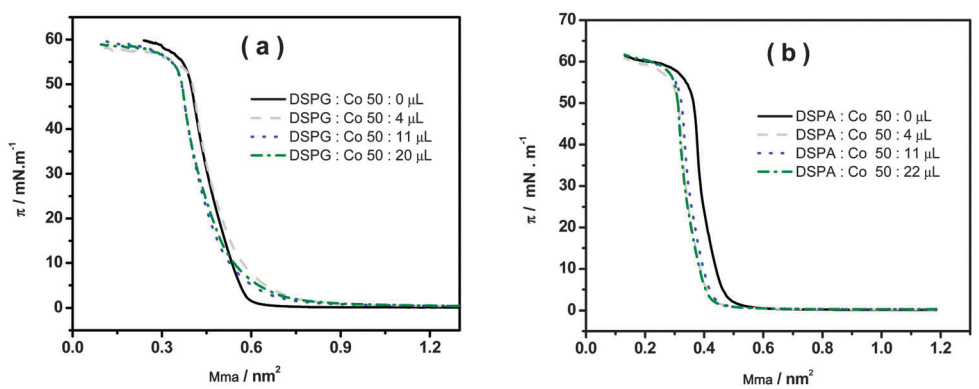

Fig. 5 Surface pressure as a function of mean molecular area (Mma) for the mixtures: (a) DSPG : Co (50 : *x* μL) and (b) DSPA : Co (50 : *x* μL). Subphase composition: 10 mM $CaCl_2$.

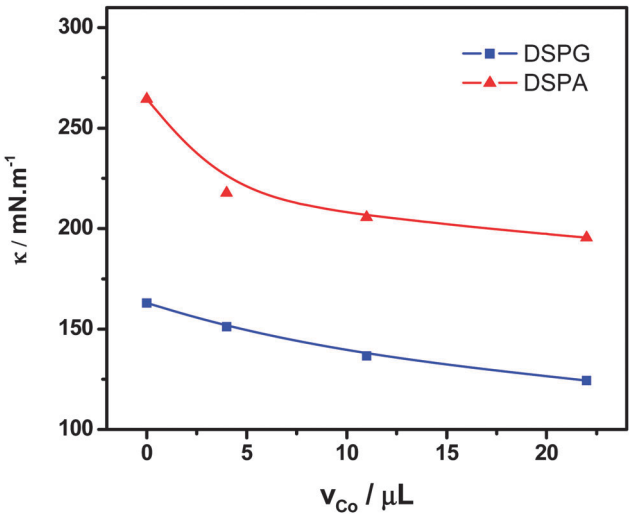

Fig. 6 Compression modulus (κ) at π = 30 mN m^{-1} *vs.* volume of Co MNPs suspension in the mixtures: DSPG:Co or DSPA:Co.

activity since no isotherms could be obtained upon injection of pure Co MNP solutions at the surface.

Fig. 6 shows the variation of the surface compression modulus κ (mN m^{-1}), calculated from the compression isotherms using eqn (1), as a function of the amount Co MNPs added to the phospholipid solutions. The decrease observed in κ reveals the formation of more expanded monolayers with lower molecular cohesion than those corresponding to pure phospholipids, with increasing the amount of nanoparticles in the mixture spread. These changes in κ values are in agreement with the enhancement of monolayer permeability observed in CV experiments in the presence of Co MNPs.

4. Conclusions

The presence of Co MNPs in DSPA or DSPG films decreases their structuration and increases their permeability to ion transfer. This effect is more pronounced in the case of DSPG films, due to the fact that DSPA forms very tightly compact films.

The DSPA:Co hybrid films are homogeneous, while the incorporation of Co MNPs into DSPG films generates domains with covered zones and pore structures. These differences in the hybrid film properties could explain the changes in permeability observed in both cases.

A decrease in the compressibility factor has been found for mixed monolayers with respect to pure phospholipids. This result supports the fact that the presence of MNPs disorganizes the lipid monolayer. The large size of the nanoparticles compared to phospholipid molecules probably contributes to the disruption of the monolayer.

Acknowledgements

Financial support from CONICET, FONCyT, SECyT-UNC and 13/ERC/12561 is gratefully acknowledged. Authors thank to M. Venkatesam for the SQUID measurements.

References

1 Q. Zhang, X. Chen, Y. Tang, L. Ge, B. Guo and C. Yao, Amperometric carbohydrate antigen 19-9 immunosensor based on three dimensional ordered macroporous magnetic Au film coupling direct electrochemistry of horseradish peroxidase, *Anal. Chim. Acta*, 2014, **815**, 42–50.
2 S. Gil and J. F. Mano, Magnetic composite biomaterials for tissue engineering, *Biomater. Sci.*, 2014, **2**, 812–818.
3 C. S. S. R. Kumar and F. Mohammad, Magnetic nanomaterials for hyperthermia-based therapy and controlled drug delivery, *Adv. Drug Delivery Rev.*, 2011, **63**, 789–808.
4 S. Amiri and H. Shokrollahi, The role of cobalt ferrite magnetic nanoparticles in medical science, *Mater. Sci. Eng., C*, 2013, **33**, 1–8.
5 J. Rivas, M. Bañobre-López, Y. Piñeiro-Redondo, B. Rivas and M. A. López-Quintela, Magnetic nanoparticles for application in cancer therapy, *J. Magn. Magn. Mater.*, 2012, **324**, 3499–3502.
6 B. Drašler, D. Drobne, S. Novak, J. Valant, S. Boljte, L. Otrin, M. Rappolt, B. Sartori, A. Iglič, V. Kralj-Iglič, V. Šuštar, D. Makovec, S. Gyergyek, M. Hočevar, M. Godec and J. Zupanc, Effects of magnetic cobalt ferrite nanoparticles on biological and artificial lipid membranes, *Int. J. Nanomed.*, 2014, **9**, 1559–1581.
7 P. B. Santhosh, S. I. Kiryakova, J. L. Genova and N. P. Ulrih, Influence of iron oxide nanoparticles on bending elasticity and bilayer fluidity of phosphotidylcholine liposomal membranes, *Colloids Surf., A*, 2014, **460**, 248–253.
8 T. J. Matshaya, A. E. Lanterna, A. M. Granados, R. W. M. Krause, B. Maggio and R. V. Vico, Distinctive interactions of oleic acid covered magnetic nanoparticles with saturated and unsaturated phospholipids in langmuir monolayers, *Langmuir*, 2014, **30**, 5888–5896.
9 M. C. Martins, C. M. Pereira, H. A. Santos, R. Dabirian, F. Silva, V. Garcia-Morales and J. A. Manzanares, Analysis of adsorption of phospholipids at the 1,2-dichloroethane/water interface by electrochemical impedance spectroscopy: A study of the effect of the saturated alkyl chain, *J. Electroanal. Chem.*, 2007, **599**, 367–375.
10 H. A. Santos, V. García-Morales, L. Murtomäki, J. A. Manzanares and K. Kontturi, Preparation of nanostructures composed of dextran sulfate/ruthenium nanoparticles and their interaction with phospholipid monolayers at a liquid–liquid interface, *J. Electroanal. Chem.*, 2007, **599**, 194–202.
11 C. I. Cámara and L. M. Yudi, Potential-mediated interaction between dextran sulfate and negatively charged phospholipids films at air/water and liquid/liquid interfaces, *Electrochim. Acta*, 2013, **113**, 644–652.
12 C. I. Cámara, M. V. C. Quiroga, N. Wilke, A. Jimenez-Kairuz and L. M. Yudi, Effect of chitosan on distearoylphosphatidylglycerol films at air/water and liquid/liquid interfaces, *Electrochim. Acta*, 2013, **94**, 124–133.
13 C. I. Cámara, L. M. A. Monzón, J. M. D. Coey and L. M. Yudi, Assambly of Magnetic nanoparticles at liquid/liquid interface.

Catalitic effect on ion transfer process, *Phys. Chem. Chem. Phys.*, submitted.

14 L. M. A. Monzón and L. M. Yudi, Cation adsorption at a distearoylphosphatidic acid layer adsorbed at a liquid/liquid interface, *Electrochim. Acta*, 2007, **52**, 6873–6879.

15 M. V. Colqui Quiroga, L. M. A. Monzón and L. M. Yudi, Interaction of triflupromazine with distearoylphosphatidylglycerol films studied by surface pressure isotherms and cyclic voltammetry at a 1,2-dichloroethane/water interface, *Electrochim. Acta*, 2010, **55**, 5840–5846.

16 M. V. Colqui Quiroga, L. M. A. Monzón and L. M. Yudi, Voltammetric study and surface pressure isotherms describing Flunitrazepam incorporation into a distearoylphosphatidic acid film adsorbed at air/water and water/1,2-dichloroethane interfaces, *Electrochim. Acta*, 2011, **56**, 7022–7028.